# Synthesis and Preclinical Evaluation of $^{11}$C-UCB-J as a PET Tracer for Imaging the Synaptic Vesicle Glycoprotein 2A in the Brain

Nabeel B. Nabulsi*[1], Joël Mercier*[2], Daniel Holden[1], Stephane Carré[2], Soheila Najafzadeh[1], Marie-Christine Vandergeten[2], Shu-fei Lin[1], Anand Deo[2], Nathalie Price[2], Martyn Wood[2], Teresa Lara-Jaime[1], Florian Montel[2], Marc Laruelle[3], Richard E. Carson[1], Jonas Hannestad[2], and Yiyun Huang[1]

[1]*Yale PET Center, New Haven, Connecticut;* [2]*UCB Biopharma, Braine-l'Alleud, Belgium; and* [3]*Intracellular Therapeutics, New York, New York*

The synaptic vesicle glycoprotein 2A (SV2A) is found in secretory vesicles in neurons and endocrine cells. PET with a selective SV2A radiotracer will allow characterization of drugs that modulate SV2A (e.g., antiepileptic drugs) and potentially could be a biomarker of synaptic density (e.g., in neurodegenerative disorders). Here we describe the synthesis and characterization of the SV2A PET radiotracer $^{11}$C-UCB-J ((*R*)-1-((3-($^{11}$C-methyl-$^{11}$C)pyridin-4-yl)methyl)-4-(3,4,5-trifluorophenyl)pyrrolidin-2-one) in nonhuman primates, including whole-body biodistribution. **Methods:** $^{11}$C-UCB-J was prepared by *C*-$^{11}$C-methylation of the 3-pyridyl trifluoroborate precursor with $^{11}$C-methyl iodide via the Suzuki–Miyaura cross-coupling method. Rhesus macaques underwent multiple scans including coinjection with unlabeled UCB-J (17, 50, and 150 μg/kg) or preblocking with the antiepileptic drug levetiracetam at 10 and 30 mg/kg. Scans were acquired for 2 h with arterial sampling and metabolite analysis to measure the input function. Regional volume of distribution ($V_T$) was estimated using the 1-tissue-compartment model. Target occupancy was assessed using the occupancy plot; the dissociation constant ($K_d$) was determined by fitting self-blocking occupancies to a 1-site model, and the maximum number of receptor binding sites ($B_{max}$) values were derived from baseline $V_T$ and from the estimated $K_d$ and the nondisplaceable distribution volume ($V_{ND}$). **Results:** $^{11}$C-UCB-J was synthesized with greater than 98% purity. $^{11}$C-UCB-J exhibited high free fraction (0.46 ± 0.02) and metabolized at a moderate rate (39% ± 5% and 24% ± 3% parent remaining at 30 and 90 min) in plasma. In the monkey brain, $^{11}$C-UCB-J displayed high uptake and fast kinetics. $V_T$ was high (~25–55 mL/cm$^3$) in all gray matter regions, consistent with the ubiquitous expression of SV2A. Preblocking with 10 and 30 mg/kg of levetiracetam resulted in approximately 60% and 90% occupancy, respectively. Analysis of the self-blocking scans yielded a $K_d$ estimate of 3.4 nM and $B_{max}$ of 125–350 nM, in good agreement with the in vitro inhibition constant ($K_i$) of 6.3 nM and regional $B_{max}$ in humans. Whole-body biodistribution revealed that the liver and the brain are the dose-limiting organs for males and females, respectively. **Conclusion:** $^{11}$C-UCB-J exhibited excellent characteristics as an SV2A PET radiotracer in nonhuman primates. The radiotracer is currently undergoing first-in-human evaluation.

**Key Words:** $^{11}$C-UCB-J; SV2A; synaptic vesicle glycoprotein; rhesus monkey; PET; epilepsy; biomarker; levetiracetam; nonhuman primate

**J Nucl Med 2016; 57:777–784**
DOI: 10.2967/jnumed.115.168179

The synaptic vesicle glycoprotein 2A (SV2A) is a transmembrane protein expressed ubiquitously in secretory vesicles in all brain areas (*1,2*). SV2A is critical for synaptic function (*3*), but the mechanisms by which SV2A regulates neurotransmitter release are unclear. Mice deficient in SV2A develop seizures and die within 3 wk of birth (*4*). In addition to its well-established role as the target for the antiepileptic drug levetiracetam (*5,6*), dysfunction of SV2A has been implicated in other neurologic disorders such as Alzheimer's disease (*7–9*).

PET imaging can be used to measure differences in the density of a molecular target under various disease conditions. Therefore, PET imaging of SV2A could be used to measure brain levels of SV2A in patients with epilepsy, Alzheimer's disease, or other neurologic and psychiatric conditions in which SV2A may play a role, and potentially as a biomarker of synaptic density in neurodegenerative disorders. Radiotracer can also be used to measure a drug's binding to its target, and PET imaging of SV2A could be used to characterize binding of levetiracetam or other SV2A-targeting drugs. A PET radiotracer should have high affinity and specificity for the target and fast kinetics. Although direct radiolabeling of levetiracetam (Fig. 1) is feasible (*10*), it is likely that its affinity is too low and its brain penetration not sufficiently fast to perform well as a PET tracer. Hence, we have developed several high-affinity SV2A ligands that penetrate the brain rapidly: UCB-A, UCB-H, and UCB-J (Fig.1) (*11*). UCB-A has been radiolabeled with $^{11}$C and tested in mini-pigs (*12*), rats (*13*), and rhesus monkeys (Nabulsi et al., unpublished data, 2012) but showed slow kinetics (prolonged retention in brain tissue) and may therefore not be suitable for PET imaging (unpublished data). UCB-H was radiolabeled with $^{18}$F and displayed good kinetics in rats (*14*) and nonhuman primates (*15*) and acceptable dosimetry in humans (*16*); however, its radiosynthesis has proven challenging and specific binding was relatively low. In this study, we report the radiosynthesis and characterization of $^{11}$C-UCB-J as a best-in-class SV2A PET tracer.

Received Oct. 13, 2015; revision accepted Dec. 25, 2015.
For correspondence or reprints contact: Nabeel Nabulsi, Yale PET Center, P.O. Box 208048, New Haven, CT 06520.
E-mail: nabeel.nabulsi@yale.edu
*Contributed equally to this work.
Published online Feb. 4, 2016.
COPYRIGHT © 2016 by the Society of Nuclear Medicine and Molecular Imaging, Inc.

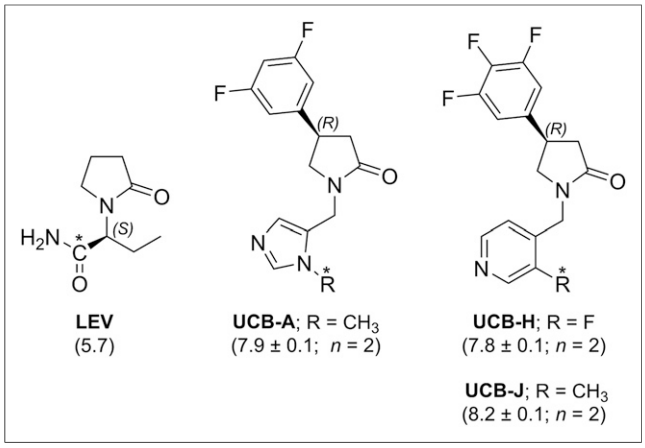


**FIGURE 1.** Representative SV2A ligands and corresponding human SV2A $pIC_{50}$ (*11*) compared with levetiracetam (LEV) $pIC_{50}$ (*19*). $pIC_{50}$ is the negative log of the $IC_{50}$ value in molar units. $pIC_{50} = -\log10(IC_{50})$, where $IC_{50}$ is half maximal inhibitory concentration. *Radiolabeling site.

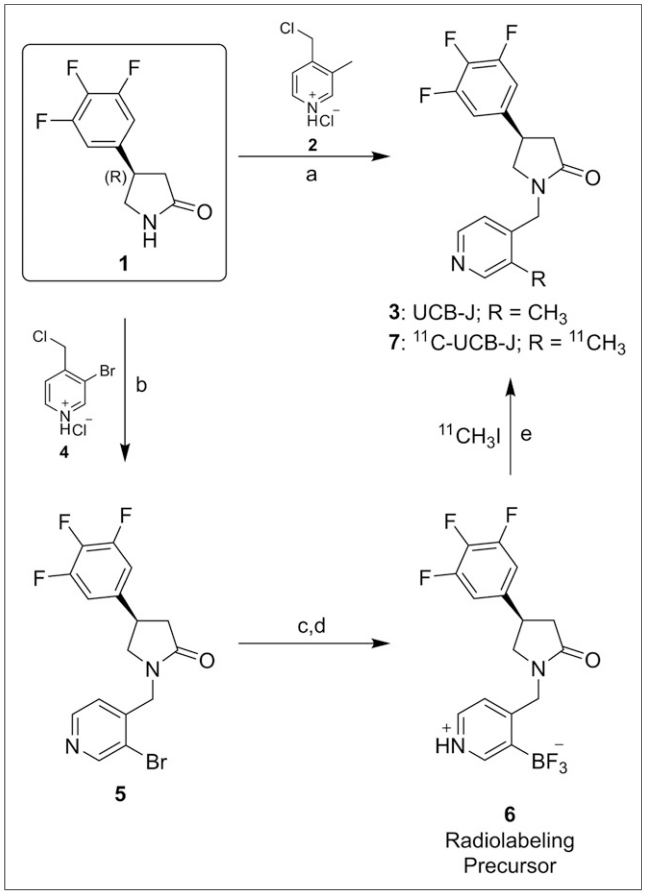


**FIGURE 2.** Synthesis of UCB-J, $^{11}$C-UCB-J, and the radiolabeling precursor: a. KI, NaH, THF, 50°C; b. NaH, THF, 50°C; c. Bis(neopentyl glycolato)diboron, $Pd(dppf)Cl_2$, AcOK, dioxane, 110°C; d. $KHF_2$, r.t.; e. $Pd_2(dba)_3$/(*o*-tolyl)$_3$P, $K_2CO_3$, DMF/$H_2O$, 100°C, 5 min.

## MATERIALS AND METHODS

### Chemistry

Figure 2 depicts a brief synthesis scheme for the preparation of the unlabeled UCB-J reference standard (**3**), the trifluoroborate radiolabeling precursor (**6**), and the radiolabeled tracer (**7**). Both the precursor and the reference standard were prepared from commercially available or custom-synthesized starting materials. Details are described in the supplemental materials (available at http://jnm.snmjournals.org).

### In Vitro Binding Assays

Binding assays were performed as previously described (*17–19*). The selectivity of UCB-J was assessed by its ability to interact with various receptors, transporters, enzymes, and ion channels (>55 targets) when tested at a concentration of 10 μM. Details are described in the supplemental materials.

### In Vitro and In Vivo Metabolism in Rats

Studies characterizing the pharmacokinetics, distribution, and metabolism of UCB-J included in vitro experiments, in vivo plasma pharmacokinetics, brain distribution, and metabolite profiling in rat plasma and brain are summarized in Table 1. Details are described in the supplemental materials. UCB-J metabolites were detected and identified using an ultraperformance liquid chromatography tandem mass spectrometry system.

### Radiochemistry

$^{11}$C-UCB-J was synthesized as previously reported (Fig. 2) (*20*). The radioligand was purified by reversed-phase high-performance liquid chromatography and formulated in 10 mL of normal saline containing 1 mL of ethanol. Details are described in the supplemental materials.

### PET Imaging Experiments in Rhesus Monkeys

*General PET Study Design.* Experiments were performed in rhesus monkeys (*Macaca mulatta*) according to a protocol approved by the Yale University Institutional Animal Care and Use Committee. Three sets of scans were obtained: baseline scan with $^{11}$C-UCB-J, followed by a blocking scan after administration of levetiracetam at a dose of 10 ($n = 2$) or 30 mg/kg ($n = 1$); in vivo maximum number of receptor binding sites ($B_{max}$)/dissociation constant ($K_d$) studies with coinjection of $^{11}$C-UCB-J and its unlabeled form at mass doses of 17, 50, and 150 μg/kg ($n = 1$ each), targeting approximately 25%, 50%, and 75% SV2A occupancy; and whole-body biodistribution scans ($n = 2$ males and 2 females).

*PET Scans and Image Analysis Procedures.* Rhesus macaques were sedated using ketamine and glycopyrrolate approximately 2 h before the first PET scan and kept anesthetized using isoflurane (1.5%–2.5%) for the duration of the experiments.

PET images of the brain were acquired using the FOCUS 220 PET scanner (Siemens Preclinical Solutions) with a reconstructed image resolution of approximately 1.5 mm. After a transmission scan, $^{11}$C-UCB-J was injected intravenously as a 3-min slow bolus by an infusion pump (PHD 22/2000; Harvard Apparatus). List-mode data were acquired for 120 min and binned into sinograms with the following frame timing: 6 × 30 s, 3 × 1 min, 2 × 2 min, and 22 × 5 min.

Scan data were reconstructed with a Fourier rebinning/filtered backprojection algorithm with corrections for attenuation, scanner normalization, radiation scatter, and randoms. Regions of interest were manually delineated on a single representative anatomic rhesus monkey MR image registered to a template image. The regions used in this study were amygdala, brain stem, caudate, cerebellum, cingulate cortex, frontal cortex, globus pallidus, insula, nucleus accumbens, occipital cortex, pons, putamen, substantia nigra, temporal cortex, and thalamus. Registration parameters were obtained to apply the regions of interest to individual PET scans (*21*), and regional time–activity curves were generated.

For the biodistribution scans, whole-body dynamic PET scanning was performed on the Siemens mCT scanner.

*Metabolite Analysis, Arterial Input Function, and Log D Determination.* Arterial blood samples were collected to calculate the plasma input function and to determine the unmetabolized parent fraction using the automatic column-switching high-performance liquid chromatography

**TABLE 1**
Summary of Studies for Pharmacokinetics, Distribution, and Metabolism in Animals

| Study type | Duration | Route of administration | Dose or concentration |
|---|---|---|---|
| Studies in rats | | | |
| Preliminary pharmacokinetics | Single dose | Intravenous | 1 mg/kg |
| Distribution (brain exposure) | Single dose | Intravenous | 0.1 mg/kg |
| Distribution and metabolism in plasma and brain | Single dose | Intravenous | 1 mg/kg |
| In vitro studies | | | |
| Brain and plasma protein binding (interspecies) | | | 1 μM |
| In vitro permeation through the caco-2 cell model | | | 2 μM |
| Intrinsic clearance in microsomes (interspecies) | | | 1 μM (rhesus), 5 μM (mouse, rat, and human) |
| Metabolism in microsomes (interspecies) | | | 1 μM |

system (*22*). Plasma free fraction ($f_p$) was measured in triplicate using the ultrafiltration method, and the log *D* was determined by modification of the previously published procedure (*23*). Additional details are provided in the supplemental materials.

*Data Analysis.* Regional time–activity curves of the brain were analyzed with the 1-tissue- (1T) compartment model. Fit quality was compared with the 2-tissue model and the multilinear analysis method (*24*) to calculate $V_T$. For the blocking and displacement experiments, target occupancy was determined using the occupancy plot (*25*).

For the whole-body scans, decay correction was removed from the time–activity curves to reflect actual radioactivity in each organ, with cumulative radioactivity ($Bq \cdot h/cm^3$) computed as the integral of the data from the scan, using physical decay to add the tail portion after the scan period.

## RESULTS

### Chemistry

Synthesis details of both UCB-J (**3**) and the radiolabeling precursor (**6**) (Fig. 2) are described in the supplemental materials.

### In Vitro Binding

In radioligand binding studies at 37°C, UCB-J displayed high SV2A binding affinity: p$K_i$ of 8.15 (7 nM) for humans and 7.6 (25 nM) for rats. As listed in Table 2, UCB-J exhibited a greater than 10-fold and greater than 100-fold selectivity for SV2A over SV2C and SV2B protein, respectively. Moreover, UCB-J at 10 μM lacked any significant interaction (<50% inhibition) with a wide variety of receptors, ion channels, enzymes, and transporters (Table 3). UCB-J is therefore a potent and selective SV2A ligand.

**TABLE 2**
Affinity of UCB-J for SV2 Proteins at 37°C

| Assay/target | p$K_i$* |
|---|---|
| Human SV2A | 8.15 ± 0.13 (4) |
| Human SV2B | 5.70 ± 0.01 (3) |
| Human SV2C | 7.00 ± 0.20 (4) |
| Rat SV2A | 7.6 (2) |

*Results are mean ± SD from (*n*) separate determinations.

### In Vitro Permeability Measurement, In Vivo Distribution, and Metabolism in Rats

In the caco-2 assay, the apparent permeability ($P_{app}$) values for UCB-J were 323 and 246 nm/s, in the A > B and the B > A assays, respectively, confirming high cell membrane permeability and absence of active transport.

In rats, UCB-J rapidly distributed into the brain in an unrestricted manner, which is consistent with its high blood–brain barrier permeability. Brain concentrations were maximal at 5 min after the dose and rapidly equilibrated with plasma concentrations. Total brain-to-plasma ratios were 8.7, 8, and 12 at 5, 10, and 20 min, respectively. Free brain-to-plasma UCB-J ratios ranged from 1.1 to 1.6 without obvious evidence of active transport. The fraction unbound to plasma proteins was investigated at 1 μM and found to be 33% and 31% in rat and human plasma, respectively. The fraction unbound in rat brain homogenate varied with the concentration, ranging from 3% to 9%.

In rats, UCB-J was rapidly eliminated, with a high total plasma clearance (30 ± 10 mL/min/kg) consistent with the medium-to-high in vitro intrinsic clearance observed in the mouse (39 μL/min/mg protein), rat (46 μL/min/mg protein), monkey (82 μL/min/mg protein), and human (16 μL/min/mg protein). On the basis of mass spectrometry response, the parent compound UCB-J was the major component detected in rat plasma and brain.

**TABLE 3**
Inhibition (%) of Radioligand Binding* to Selected Targets

| Target | $H_1$ | $\alpha_{2A}$ | $\alpha_{1A}$ | $M_2$ | $\delta_1$ | κOR | $D_2$ | 5-$HT_{1A}$ | 5-$HT_{2A}$ |
|---|---|---|---|---|---|---|---|---|---|
| % inhibition | 3 | 7 | −4 | 2 | 4 | 3 | 2 | −2 | 3 |

*Performed in duplicate at concentrations of 10 μm.

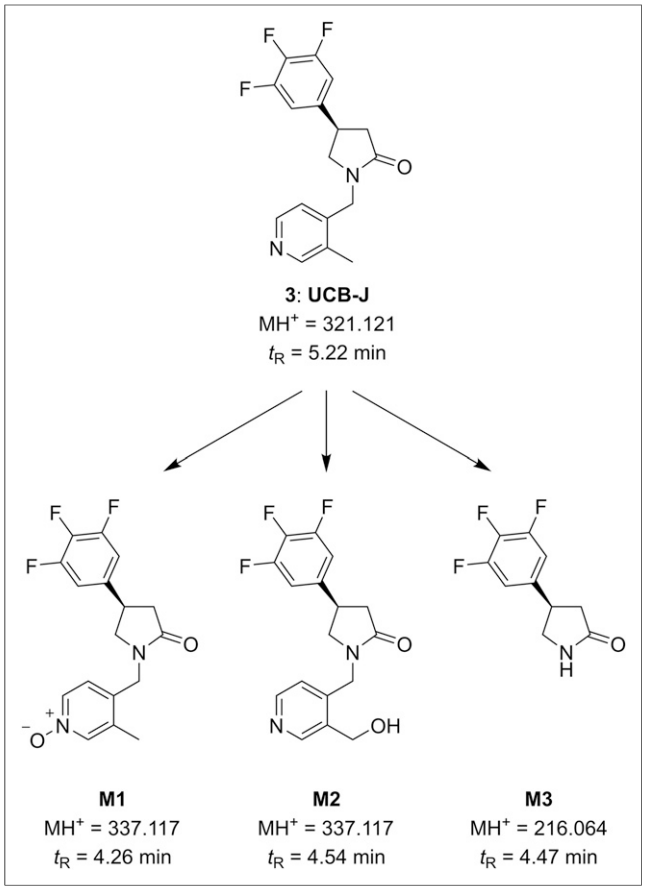


**FIGURE 3.** Metabolic pathways in rat plasma after single intravenous dose of UCB-J (1 mg/kg).

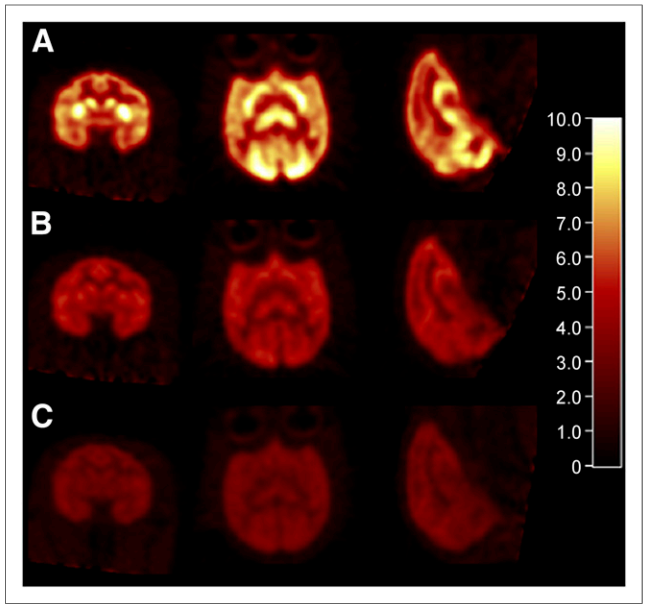


**FIGURE 4.** Representative SUV images summed from 30 to 45 min after $^{11}$C-UCB-J injections: baseline (A), after pretreatment with levetiracetam (10 mg/kg) (B), and after coinjection with unlabeled UCB-J (150 μg/kg) (C).

The metabolic clearance of UCB-J occurred by 3 major pathways as shown in Figure 3: *N*-oxidation (M1), methyl hydroxylation (M2), and *N*-dealkylation of the pyrrolidinone ring (M3). M1, M2, and M3 were found at 16.9%, 7.7%, and 1.3% (percentage of total detected material), respectively, from the 0- to the 2-h period.

In the rat brain, M1 and M2 were the only metabolites observed at trace levels (0.1% and 1.3%, respectively, average for the 0- to 2-h collection period). Qualitative mass spectrometry evaluation of the interspecies metabolism suggested that the metabolic clearance of UCB-J occurred primarily by hydroxylation on the methyl pyridine ring. No unique human metabolite was observed, suggesting that the metabolites observed in humans should be the same as those in rats. Overall, these data suggest that the circulating metabolites are polar and thus not likely to cross the blood–brain barrier.

### Radiochemistry

$^{11}$C-UCB-J was produced from 1 mg of precursor in a radiochemical yield of 11% ± 4% (based on trapped $^{11}$C-methyl iodide radioactivity), with a radiochemical purity of 99% ± 0.5%, chemical purity of 99.8% ± 2.4%, and specific activity of 566.1 ± 266 MBq/nmol at the end of synthesis ($n$ = 16). The stability of $^{11}$C-UCB-J was evaluated at 150 min after the end of synthesis, with the radiochemical purity maintained at 99% or greater. Further details are reported in the supplemental materials.

### PET Scans in Rhesus Monkeys

For the brain imaging study, the injected dose of $^{11}$C-UCB-J was 141 ± 42 MBq, with a specific activity of 252 ± 151 MBq/nmol at the time of injection ($n$ = 11), and injected mass was 0.05 ± 0.04 μg/kg ($n$ = 8). For the dosimetry scans, the injected radioactivity dose was 170 ± 15 MBq, with a specific activity of 371 ± 42 MBq/nmol at the time of injection and injected mass dose of 0.02 ± 0.01 μg/kg ($n$ = 4).

*In Vivo Metabolite Analysis in Monkeys.* $^{11}$C-UCB-J displayed fairly fast metabolism in Rhesus monkeys. The parent fraction in the plasma accounted for approximately 40% and about 25% of the radioactivity at 30 and 90 min after injection, respectively. The primary metabolite peak was more polar than the parent (retention time of ~7 min, compared with ~11 min for the parent compound). The $f_p$ was high, at 46.2% ± 2.5% ($n$ = 11). The measured log $D$ of $^{11}$C-UCB-J was 2.53 ± 0.02 (range, 2.46–2.56), in the optimal range for brain PET radiotracers.

*Image Analysis and Kinetic Modeling.* Representative PET images of $^{11}$C-UCB-J are shown in Figure 4. At baseline, high uptake was seen throughout the gray matter, consistent with the ubiquitous distribution of SV2A in the brain (Fig. 4A). Blockade of $^{11}$C-UCB-J binding by levetiracetam (Fig. 4B) and coinjected UCB-J (Fig. 4C) was evident in the images, as indicated by decreased activity levels.

Regional time–activity curves are presented in Figure 5. In the monkey brain $^{11}$C-UCB-J displayed a high uptake and rapid kinetics, with an $SUV_{peak}$ of 5–8 in gray matter areas and peak uptake times ranging from 10 to 50 min (Fig. 5A). When the animal was pretreated with 10 mg/kg of levetiracetam, activity concentrations in brain regions peaked earlier and cleared faster

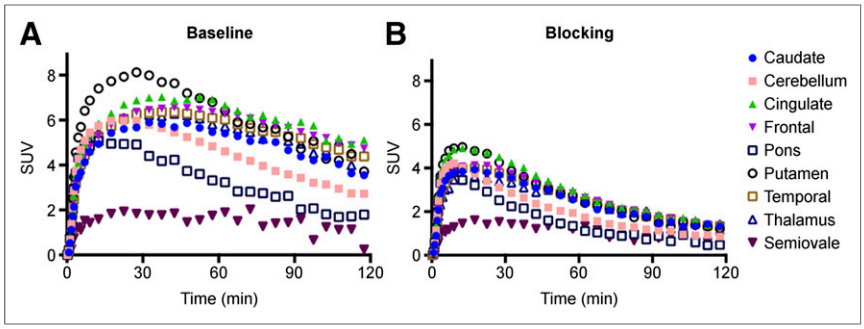


**FIGURE 5.** Time–activity curves in selected brain regions from $^{11}$C-UCB-J baseline (A) and blocking (B) scans after pretreatment with levetiracetam (10 mg/kg).

(Fig. 5B), demonstrating substantial blockade of $^{11}$C-UCB-J binding by the drug.

The 1T model produced reliable $V_T$ estimates (low SE) with suitable fits. Multilinear analysis produced good fits with small differences in $V_T$ values from 1T (supplemental materials). Overall, the 2-tissue model produced $V_T$ estimates with high SE. Thus, the 1T model was the chosen method for analysis.

Regional $V_T$ values are listed in Table 4. The highest values are in the cortical areas; moderate in the caudate, putamen, and thalamus; and lower in other regions. Significant reduction in regional $V_T$ was seen with the administration of levetiracetam (10 and 30 mg/kg). In the self-blocking scans with UCB-J, a clear dose-dependent reduction in regional $V_T$ was observed, as depicted in Figure 6. Receptor occupancy calculated from the occupancy plots was 59% and 89% for the 10 and 30 mg/kg doses of levetiracetam, respectively. Occupancies of 46%, 68%, and 87% were found with self-blocking doses of 17, 50, and 150 μg/kg UCB-J.

*Determination of In Vivo $K_d$ and $B_{max}$.* Estimates of $K_d$ and $B_{max}$ were determined from baseline $V_T$ and receptor occupancy data from the self-blocking experiments. Figure 7 depicts the $K_d$ estimation by fitting the receptor occupancy (*RO*) measurements as a function of free tracer concentration in plasma ($C_{PF}$), computed as the average metabolite-corrected plasma values from 60 to 120 min, multiplied by $f_p$, as follows:

$$RO = C_{PF}/(C_{PF} + K_d)$$

The estimated value of $K_d$ was 3.4 ± 0.2 nM. To determine $B_{max}$, the nondisplaceable distribution volume ($V_{ND}$) was first estimated from the x-intercept of the occupancy plots from 6 blocking scans (3 with levetiracetam and 3 with UCB-J) and determined to be 6.27 ± 0.60 mL/cm$^3$. Then, $B_{max}$ (nM) was computed as

$$B_{max} = K_d^*(V_{T\ Baseline} - V_{ND})/f_p$$

Estimates of $B_{max}$ and $K_d$ values are included in Table 4.

*Dosimetry.* Visual evaluation of dosimetry scans detected early uptake in the liver and brain. Mid-scan uptake occurred in the kidneys and urinary bladder, with radioactivity remaining in the brain and liver. At the end of the scan, radioactivity was seen in

**TABLE 4**
Regional Binding Parameters for $^{11}$C-UCB-J at Baseline and After Preblocking with Levetiracetam

| Brain region | Baseline $V_T$ ($n$ = 5) | Preblocking $V_T$ with dose of levetiracetam* | | $B_{max}$† (nmol/L) |
|---|---|---|---|---|
| | | 10 mg/kg ($n$ = 2) | 30 mg/kg ($n$ = 1) | |
| Amygdala | 23.42 (1.3) | 11.89 (0.5) | 7.25 | 128 |
| Brain stem | 22.90 (2.0) | 11.83 (0.3) | 8.98 | 124 |
| Caudate | 43.39 (4.0) | 19.71 (0.2) | 11.53 | 276 |
| Cerebellum | 34.80 (3.8) | 15.85 (0.9) | 10.59 | 212 |
| Cingulate cortex | 53.41 (7.7) | 22.68 (0.6) | 12.79 | 350 |
| Frontal cortex | 52.96 (6.5) | 21.32 (0.3) | 11.49 | 347 |
| Globus pallidus | 27.13 (2.0) | 16.01 (0.6) | 11.3 | 155 |
| Insula | 52.45 (5.2) | 22.47 (0.3) | 12.97 | 343 |
| Nucleus accumbens | 51.63 (6.5) | 24.12 (1.2) | 13.39 | 337 |
| Occipital cortex | 50.85 (5.0) | 20.14 (0.1) | 11.8 | 331 |
| Pons | 22.78 (2.3) | 11.50 (0.7) | 9.3 | 123 |
| Putamen | 43.95 (1.9) | 20.40 (1.0) | 12.39 | 280 |
| Substantia nigra | 23.98 (2.2) | 12.60 (0.2) | 9.28 | 132 |
| Temporal cortex | 48.31 (4.9) | 20.35 (0.2) | 11.88 | 313 |
| Thalamus | 38.62 (4.8) | 18.56 (1.9) | 11.09 | 241 |

*Values in parentheses are SDs.
†$B_{max}$ values calculated from baseline $V_T$ values correcting for $V_{ND}$, derived form 6 occupancy scans and using mean $f_P$ value.

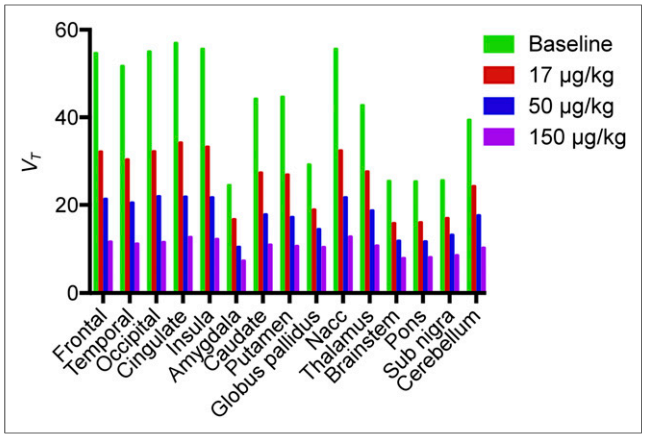


**FIGURE 6.** Bar graph representation of $^{11}$C-UCB-J self-blocking scans after coadministration of UCB-J (17, 50, and 150 µg/kg).

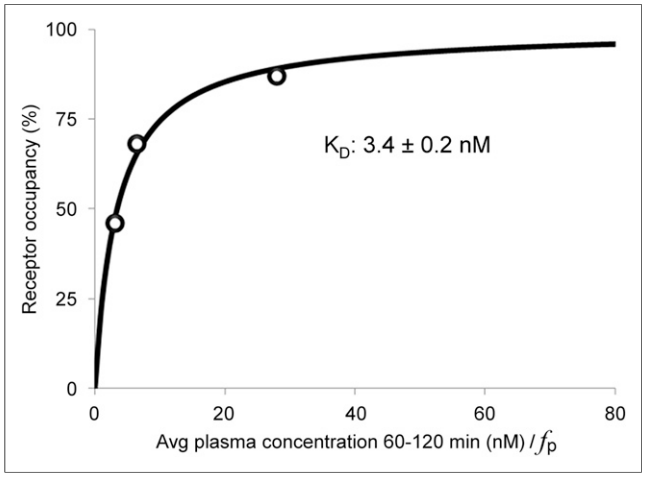


**FIGURE 7.** In vivo $K_d$ estimate for UCB-J from 1T $V_T$ values. Avg = average.

the urinary bladder and gallbladder, with less remaining in the kidney and liver. Absorbed doses derived from the 70-kg reference male and 55-kg adult female phantoms are shown in Table 5. The liver is the dose-limiting organ, with a single-study dose limit of 2,500 MBq (68 mCi) for a male, whereas the brain is the dose-limiting organ for the female, with a single-study dose limit of approximately 2,750 MBq (75 mCi).

## DISCUSSION

In this report, we describe the synthesis and evaluation of a novel radiotracer for SV2A. Radiosynthesis of $^{11}$C-UCB-J involved the Suzuki–Miyaura cross-coupling of the 3-pyridyl trifluoroborate precursor with $^{11}$C-$CH_3$I, which produced $^{11}$C-UCB-J in good yield and high chemical/radiochemical purity. To the best of our knowledge, this is the first report for the use of trifluoroborate in $^{11}$C radiolabeling. This is also the second report for the successful use of 1 mg of precursor in the cross-coupling reaction, rather than 2 mg or more, which is usually used. The 3-pyridyl boronic acid precursor also underwent efficient *C*-$^{11}$C-methylation to give $^{11}$C-UCB-J. However, the protodeborylated product, which possesses affinity appreciable to SV2A (p*K*i = 8.0 ± 0.1) was always detected in the final product when the boronic acid precursor was used, but not present with the use of the trifluoroborate precursor. It is unclear whether this deborylated product is formed as a side reaction during the radiolabeling of the boronic acid precursor, which is known to occur particularly with electron-rich boronic acids (*26*), or by decomposition of the boronic acid precursor during work-up. Both base- and metal-catalyzed deboronation of boronic acids may occur under typical Suzuki–Miyaura cross-coupling reaction conditions (*27,28*).

Evaluation in rhesus monkeys showed that $^{11}$C-UCB-J displays excellent pharmacokinetic and imaging characteristics: brain uptake is high, with an $SUV_{peak}$ of 5–8 in gray matter regions, leading to high-quality PET images; tissue kinetics are appropriate for an $^{11}$C tracer; $f_p$ is high, and thus can be reliably measured; time–activity curves are well fitted by the 1T model to produce stable measures of regional $V_T$; and saturable and specific binding for SV2A is demonstrated by dose-dependent blockade with levetiracetam and unlabeled UCB-J.

As expected from the ubiquitous expression of SV2A in the brain, binding of $^{11}$C-UCB-J was seen in all gray matter areas, with high $V_T$ in cortical areas and lower in other regions. The lowest $V_T$ was found in the centrum semiovale (white matter), consistent with ex vivo autoradiography findings in the spinal cord (*29*). Therefore, we evaluated the potential utility of white matter as a reference region by analysis of the 4 scans from the self-blocking (in vivo $K_d$) study. Because of the high gray/white contrast, partial-volume correction was performed (supplemental materials). The corrected white matter $V_T$ values showed a minimal effect of unlabeled UCB-J and were in the range of 6–7 mL·cm$^{-3}$, which is in excellent agreement with the $V_{ND}$ value determined from the occupancy plots (6.3 ± 0.6 mL·cm$^{-3}$). These results support the lack of specific SV2A binding in white matter. Thus, white matter may serve as a suitable reference region in kinetic analysis, without the need for arterial input function measurement.

The measured in vivo $K_d$ value of $^{11}$C-UCB-J in this study (3.4 ± 0.2 nM) is in good agreement with the reported in vitro inhibition constant ($K_i$) value of 6.3 nM for human SV2A (*11*). Furthermore, the estimated regional density ($B_{max}$) for neuronal SV2A protein in this study is 125–350 nM, which also is in close agreement with the reported regional $B_{max}$ values in the human brain measured in vitro (*5*).

In preparation for the use of $^{11}$C-UCB-J in humans, we performed whole-body distribution studies in rhesus monkeys to calculate organ radiation dosimetry. The organs receiving the largest dose were the liver for males (0.0199 mGy/MBq or 0.0735 rad/mCi) and the brain for females (0.0181 mGy/MBq or 0.0671 rad/mCi). The estimated effective dose equivalent (EDE) value of approximately 4.5 µSv/MBq for $^{11}$C-UCB-J EDE is in the lower range of EDE values (3.3–17.4 µSv/MBq) reported in a recent review of organ dosimetry for $^{11}$C-labeled radiotracer (*30*). Therefore, the maximum EDE from a single 740 MBq (20 mCi) administration of $^{11}$C-UCB-J is equivalent to 3.4 mSv (0.34 rem). Thus, multiple injections can be performed in healthy subjects per year.

In addition to studies with $^{11}$C-UCB-J, we also briefly evaluated $^{18}$F-UCB-H (*15*) in nonhuman primates to assess which tracer has higher specific binding ($BP_{ND}$); we compared their $V_T$ values at baseline in nonhuman primates, using a recently developed graphical method (*31*). Results indicated that $^{11}$C-UCB-J has higher $BP_{ND}$ than $^{18}$F-UCB-H (supplemental materials).

**TABLE 5**
Mean Organ Radiation Dose (mGy/MBq) Estimates from $^{11}$C-UCB-J in 70-Kilogram Adult Male and 55-Kilogram Female Phantoms

| Target organ | Male | | Female | |
|---|---|---|---|---|
| | Mean | SD | Mean | SD |
| Adrenals | 1.75E–03 | 5.73E–04 | 1.46E–03 | 2.29E–05 |
| Brain | 1.74E–02 | 4.00E–04 | 1.81E–02 | 6.89E–04 |
| Breasts | 4.27E–04 | 1.22E–04 | 3.14E–04 | 7.65E–06 |
| Gallbladder wall | 3.24E–03 | 1.45E–03 | 3.68E–03 | 9.57E–05 |
| Lower large intestine wall | 7.11E–03 | 2.64E–03 | 6.68E–03 | 8.59E–04 |
| Small intestine | 6.27E–04 | 1.22E–04 | 6.30E–04 | 3.24E–05 |
| Stomach wall | 1.14E–03 | 2.41E–04 | 1.00E–03 | 7.08E–05 |
| Upper large intestine wall | 7.59E–04 | 2.50E–04 | 7.00E–04 | 2.10E–05 |
| Heart wall | 2.29E–03 | 6.95E–04 | 1.64E–03 | 7.46E–05 |
| Kidneys | 1.26E–02 | 2.60E–03 | 1.17E–02 | 5.92E–04 |
| Liver | 1.99E–02 | 9.49E–03 | 1.69E–02 | 1.91E–04 |
| Lungs | 5.24E–03 | 1.91E–05 | 3.00E–03 | 3.05E–04 |
| Muscle | 4.46E–04 | 1.13E–04 | 4.05E–04 | 5.73E–06 |
| Ovaries | – | – | 6.43E–04 | 7.65E–05 |
| Pancreas | 1.97E–03 | 5.16E–04 | 1.54E–03 | 4.00E–04 |
| Red marrow | 7.05E–04 | 1.16E–04 | 6.62E–04 | 3.81E–06 |
| Osteogenic cells | 6.62E–04 | 8.22E–05 | 6.89E–04 | 1.34E–05 |
| Skin | 3.11E–04 | 6.16E–05 | 2.89E–04 | 1.91E–06 |
| Spleen | 3.46E–03 | 4.78E–04 | 3.59E–03 | 1.29E–03 |
| Testes | 9.59E–05 | 2.45E–05 | – | – |
| Thymus | 4.76E–04 | 1.13E–04 | 3.41E–04 | 1.34E–05 |
| Thyroid | 4.11E–04 | 1.15E–05 | 2.20E–04 | 8.59E–06 |
| Urinary bladder wall | 3.24E–03 | 2.27E–03 | 9.38E–03 | 2.01E–03 |
| Uterus | – | – | 6.22E–04 | 8.97E–05 |
| Total body | 1.44E–03 | 3.27E–04 | 1.34E–03 | 1.34E–05 |
| EDE | 4.59E–03 | 3.43E–04 | 4.46E–03 | 9.57E–05 |
| Effective dose | 3.32E–03 | 1.53E–04 | 3.35E–03 | 1.72E–04 |

## CONCLUSION

We have described the synthesis and preclinical evaluation of the novel SV2A tracer $^{11}$C-UCB-J and demonstrated its suitability as a PET tracer for quantifying SV2A protein in nonhuman primates. $^{11}$C-UCB-J displayed high regional specific binding signals in rhesus monkeys and a favorable metabolic profile with suitable brain uptake kinetics. Clinical evaluation of $^{11}$C-UCB-J is currently under way.

## DISCLOSURE

The costs of publication of this article were defrayed in part by the payment of page charges. Therefore, and solely to indicate this fact, this article is hereby marked "advertisement" in accordance with 18 USC section 1734. Research support was provided by UCB Biopharma. At the time this work was conducted, Joël Mercier, Stephane Carré, Marie-Christine Vandergeten, Anand Deo, Nathalie Price, Martyn Wood, Florian Montel, Marc Laruelle, and Jonas Hannestad were employees of UCB Biopharma. No other potential conflict of interest relevant to this article was reported.

## ACKNOWLEDGMENT

We thank the staff of the Yale PET Center for their expert assistance.

## REFERENCES

1. Bajjalieh SM, Peterson K, Shinghal R, Scheller R. SV2, a brain synaptic vesicle protein homologous to bacterial transporters. *Science.* 1992;257:1271–1273.
2. Bajjalieh SM, Frantz GD, Weimann JM, McConnell SK, Scheller RH. Differential expression of synaptic vesicle protein 2 (SV2) isoforms. *J Neurosci.* 1994;14:5223–5235.
3. Vogl C, Tanifuji S, Danis B, et al. Synaptic vesicle glycoprotein 2A modulates vesicular release and calcium channel function at peripheral sympathetic synapses. *Eur J Neurosci.* 2015;41:398–409.
4. Crowder KM, Gunther JM, Jones TA, et al. Abnormal neurotransmission in mice lacking synaptic vesicle protein 2A (SV2A). *Proc Natl Acad Sci USA.* 1999;96:15268–15273.
5. Gillard M. Binding characteristics of levetiracetam to synaptic vesicle protein 2A (SV2A) in human brain and in CHO cells expressing the human recombinant protein. *Eur J Pharmacol.* 2006;536:102–108.
6. Kaminski RM, Gillard M, Klitgaard H. Targeting SV2A for discovery of antiepileptic drugs. In: Noebels JL, Avoli M, Rogawski MA, Olsen RW, Delgado-Escueta AV, eds. *Jasper's Basic Mechanisms of the Epilepsies.* 4th ed. Bethesda, MD: National Center for Biotechnology Information (US); 2012:83.

7. Kaufman AC, Salazar SV, Haas LT, et al. Fyn inhibition rescues established memory and synapse loss in Alzheimer mice. *Ann Neurol.* 2015;77:953–971.
8. Robinson JL, Molina-Porcel L, Corrada MM, et al. Perforant path synaptic loss correlates with cognitive impairment and Alzheimer's disease in the oldest-old. *Brain.* 2014;137:2578–2587.
9. Rhinn H, Fujita R, Qiang L, Cheng R, Lee JH, Abeliovich A. Integrative genomics identifies APOE ε4 effectors in Alzheimer's disease. *Nature.* 2013;500: 45–50.
10. Cai H, Mangner TJ, Muzik O, Wang MW, Chugani DC, Chugani HT. Radiosynthesis of $^{11}$C-levetiracetam: a potential marker for PET imaging of SV2A expression. *ACS Med Chem Lett.* 2014;5:1152–1155.
11. Mercier J, Archen L, Bollu V, et al. Discovery of heterocyclic nonacetamide synaptic vesicle protein 2A (SV2A) ligands with single-digit nanomolar potency: opening avenues towards the first SV2A positron emission tomography (PET) ligands. *ChemMedChem.* 2014;9:693–698.
12. Lubberink M, Estrada S, Thibblin A, et al. Pre-clinical evaluation and kinetic modelling of 11C-UCB-A as a PET tracer for synaptic vesicle protein 2A. Abstract presented at: The 10th International Symposium on Functional NeuroReceptor Mapping of the Living Brain; May 21–24, 2014, Amsterdam, The Netherlands.
13. Estrada S, Thibblin A, Johansen P, et al. Synthesis, biodistribution and radiation dosimetry of 11C-UCB-A, a novel PET tracer for synaptic vesicle protein 2A. Abstract presented at: The 10th International Symposium on Functional NeuroReceptor Mapping of the Living Brain; May 21–24, 2014; Amsterdam, The Netherlands.
14. Warnock GI, Aerts J, Bahri MA, et al. Evaluation of $^{18}$F-UCB-H as a novel PET tracer for synaptic vesicle protein 2A in the brain. *J Nucl Med.* 2014;55:1336–1341.
15. Zheng M-Q, Holden D, Nabulsi N, et al. Synthesis and evaluation of $^{18}$F-UCB-H, a novel PET imaging tracer for the synaptic vesicle protein 2A [abstract]. *J Nucl Med.* 2014;55(suppl 1):1792.
16. Bretin F, Bahri MA, Bernard C, et al. Biodistribution and radiation dosimetry for the novel SV2A radiotracer [$^{18}$F]UCB-H: first-in-human study. *Mol Imaging Biol.* 2015;17:557–564.
17. Fuks B, Gillard M, Michel P, et al. Localization and photoaffinity labelling of the levetiracetam binding site in rat brain and certain cell lines. *Eur J Pharmacol.* 2003;478:11–19.
18. Gillard M, Fuks B, Michel P, Vertongen P, Massingham R, Chatelain P. Binding characteristics of [$^{3}$H]ucb 30889 to levetiracetam binding sites in rat brain. *Eur J Pharmacol.* 2003;478:1–9.
19. Lynch BA, Lambeng N, Nocka K, et al. The synaptic vesicle protein SV2A is the binding site for the antiepileptic drug levetiracetam. *Proc Natl Acad Sci USA.* 2004;101:9861–9866.
20. Nabulsi N, Hannestad J, Holden D, et al. [$^{11}$C]UCB-J: a novel PET tracer for imaging the synaptic vesicle glycoprotein 2A (SV2A) [abstract]. *J Nucl Med.* 2014;55(suppl 1):355.
21. Sandiego CM, Weinzimmer D, Carson RE. Optimization of PET-MR registrations for nonhuman primates using mutual information measures: a multi-transform method (MTM). *Neuroimage.* 2013;64:571–581.
22. Hilton J, Yokoi F, Dannals RF, Ravert HT, Szabo Z, Wong DF. Column-switching HPLC for the analysis of plasma in PET imaging studies. *Nucl Med Biol.* 2000; 27:627–630.
23. del Rosario RB, Jung Y-W, Baidoo KE, Lever SZ, Wieland DM. Synthesis and in vivo evaluation of a $^{99m99}$Tc-DADT-Benzovesamicol: a potential marker for cholinergic neurons. *Nucl Med Biol.* 1994;21:197–203.
24. Ichise M, Toyama H, Innis RB, Carson RE. Strategies to improve neuroreceptor parameter estimation by linear regression analysis. *J Cereb Blood Flow Metab.* 2002;22:1271–1281.
25. Cunningham VJ, Rabiner EA, Slifstein M, Laruelle M, Gunn RN. Measuring drug occupancy in the absence of a reference region: the Lassen plot re-visited. *J Cereb Blood Flow Metab.* 2010;30:46–50.
26. Soloducho J, Olech K, Swist A, Zajac D, Cabaj J. Recent advances of modern protocol for C-C bonds: the Suzuki Cross-Coupling. *ACES.* 2013;3:19–32.
27. Kuivila HG, Reuwer JF Jr, Mangravite JA. Electrophilic displacement reactions: XV—kinetics and mechanism of the base-catalyzed protodeboronation of areneboronic acids. *Can J Chem.* 1963;41:3081–3090.
28. Kuivila HG. Electrophilic displacement reactions. XVI. Metal ion catalysis in the protodeboronation of areneboronic acids. *J Am Chem Soc.* 1964;86:2666–2670.
29. Lambeng N, Gillard M, Vertongen P, Fuks B, Chatelain P. Characterization of [$^{3}$H]ucb 30889 binding to synaptic vesicle protein 2A in the rat spinal cord. *Eur J Pharmacol.* 2005;520:70–76.
30. van der Aart J, Hallett WA, Rabiner EA, Passchier J, Comley RA. Radiation dose estimates for carbon-11-labelled PET tracers. *Nucl Med Biol.* 2012;39:305–314.
31. Guo Q, Owen DR, Rabiner EA, Turkheimer FE, Gunn RN. A graphical method to compare the in vivo binding potential of PET radioligands in the absence of a reference region: application to [$^{11}$C]PBR28 and [$^{18}$F]PBR111 for TSPO imaging. *J Cereb Blood Flow Metab.* 2014;34:1162–1168.